Hindawi
International Journal of Photoenergy
Volume 2023, Article ID 7394007, 10 pages
https://doi.org/10.1155/2023/7394007

Research Article

Influence of Inclination Angle at the Chimney Inlet on the Power Generation in Solar Chimney Power Plants through 3D CFD Model

Mahmut Kaplan

Gaziantep University, Gaziantep 27600, Türkiye

Correspondence should be addressed to Mahmut Kaplan; mahmutkaplan@gantep.edu.tr

Received 8 October 2023; Revised 5 November 2023; Accepted 8 December 2023; Published 23 December 2023

Academic Editor: Qiliang Wang

The sun is an abundantly available and clean renewable energy source. Therefore, solar energy offers significant potential for mitigating climate change and reducing emissions from burning fossil fuels in the future. Solar chimney power plants (SCPPs) have a technical capability for meeting the massive sustainable power production. Basic parts of SCPP system are the chimney, turbine, and collector. The geometric dimensions of the components are the crucial factors for improving the solar chimney efficiency. The goal of this work is to analyse the influences of the inclination angle (θ) at chimney inlet on performance characteristics of the system by employing RNG $k-\varepsilon$ turbulence model coupled with discrete ordinate (DO) solar ray tracing method via ANSYS Fluent CFD software. The model is built by taking into consideration geometric parameters of Manzanares plant and verified with its measurements. The innovative chimney entrance configurations are produced by altering the chimney entrance slope ($\theta = 50^\circ$–80°) with the geometrical dimensions of the chimney, collector, and fillet keeping constant. The computational results display that the new chimney configurations improve the maximum velocity, system power output, and turbine pressure drop. The peak velocity of 18.1 m/s is gained for the configuration with $\theta = 80^\circ$ compared to that of 14.3 m/s obtained for the base model having $\theta = 45^\circ$ at 1000 W/m^2. Besides, this configuration enhances power output to 61.5 kW with a rise of 24.5% compared to the base model with a power output of 49.1 kW at 1000 W/m^2.

1. Introduction

Renewables including solar, wind, hydropower, tidal, geothermal, biomass, and wastes are of key importance to solve global challenges related to climate change and an increase in energy demand owing to high population in the future [1, 2].

Solar energy is capable of supplying safe, clean, sustainable, and plentiful energy for producing heat and electricity for a wide variety of industrial applications and buildings [3, 4]. In recent years, the solar chimney technology has been developed to meet massive energy needs from the sun [5, 6]. Basic elements of the solar chimney power plants (SCPPs) are the chimney, collector, and turbine. The chimney generates pressure difference owing to its long cylindrical shape. This leads to upward-moving air from the chimney entrance to the chimney outlet. The greenhouse effect induced by the collector with the semitransparent roof is also contributed to upward air motion towards the chimney. Namely, solar radiation transmitted to the ground throughout the transparent glass or film canopy augments temperature of the air under the collector, which causes buoyancy-driven convective flow in the solar chimney owing to density difference between cold and hot air. Besides, a variety of high thermal energy storage materials like concrete and ceramic under the collector are used to generate uninterrupted power during nighttime and cloudy-sky days. With all of the effects, the warm air moves into the chimney with fast speed. Therefore, the turbine is situated around the chimney inlet. The increased air's kinetic energy is changed into mechanical energy at the turbine and eventually into electric energy employing an appropriate generator [7].

The geometric feature variations of the solar chimney parts influence the flow and output power in the SCPP

system [8–13]. The height and radius of the collector and chimney are basic dimensions of the plant. In addition, the divergent and convergent solar chimney shapes influence performance characteristics of the solar chimney. Recently, several research works have been conducted on the impacts of various chimney shapes on air fluid behaviour and the plant efficiency. Nasraoui et al. [14] analysed the impact of various chimney configurations including cylindrical (small and wide) and divergent (conical and hyperboloid) chimneys with different DR ratio (outlet diameter/inlet diameter) on fluid flow characteristics and performance of SCPP by using ANSYS Fluent. They found that the solar chimney efficiency augmented chimneys with divergent geometry and the highest power output was provided with hyperboloid shape chimney configuration for DR = 8. It was also shown that velocity distribution along the chimney length was more uniform with the small diameter chimney in comparison with the large diameter case. Cuce et al. [15] investigated the impacts of various chimney configurations generated by changing the outlet radius of the chimney with fixed for various AR (outlet area of chimney divided by inlet area of chimney) ranging between 0.5 and 10. Their results obtained with RNG $k-\varepsilon$ turbulence model demonstrated that the case with AR = 4.1 elevated the SCPP efficiency of 0.83% at the highest power output of 168.5 kW compared to the prototype plant in Spain. Besides, Cuce et al. [16] performed the effect of the slenderness (height of chimney/diameter of chimney) ranging between 3 and 40 on performance characteristics of the system utilizing same turbulence model in ANSYS Fluent software. Their results illustrated that the configuration with the slenderness value of 8 provided the highest power output and elevated efficiency considerably compared to reference case built on the Manzanares plant.

The existence of a fillet before the chimney inlet has a vital role in the direction of the airflow in the solar chimney. The modification of the fillet geometry influences the flow field structure of the chimney entrance. An efficient fillet shape is required to improve flow acceleration around the turbine. Aziz and Elsayed [17] suggested six different fillet configurations to enhance flow field at the chimney entrance. Their findings indicated that the flow separation has a major effect to augment air velocity at the chimney inlet. Praveen [18] established a 3D solar chimney model using the dimensions of the Spanish plant to examine the impact of various fillet sizes (0.5 m-3 m) having a fixed angle of 45° at the chimney base on the power production features of the plant. The results indicated that the configuration with a 2.5 m depth of the fillet significantly augmented the maximum average velocity, pressure drop, and output power, and thus the plant efficiency compared to other fillet shapes and the no-fillet case.

Based on the available literature, the main conclusions are that there are many numerical works related to the impacts of the primary dimensions (height and width) of the plant on the flow and performance features of the solar chimney system, but there is no sufficient information available about the chimney entrance dimension impact on the efficiency of power production of the system. The current work is unique in that it aims to establish a 3D CFD model to assess the influence of the different chimney inlet geometries generated by changing inclination angle θ (50°–80°) on power production of the SCPPs. Modification of θ at the chimney entrance can provide an opportunity to induce high velocity near the chimney base. The current work answers this gap. Therefore, the CFD results will make an original contribution to improving the solar chimney design to maximize output power.

Table 1: The CFD model dimensions [19].

Geometrical parameters	Value
Roof height	1.85 m
Roof radius	122 m
Chimney height	194.6 m
Chimney radius	5.08 m

2. Materials and Methods

2.1. Modeling of SCPP. Performance analysis of the SCPP is conducted using the fundamental dimensions of the Manzanares plant in Table 1.

The thicknesses of the ground, collector, and chimney are 0.5, 0.004, and 0.00125 m, respectively [20]. Three-dimensional (3D) computational model is produced in ANSYS DesignModeler. Figure 1(a) demonstrates the sketch of the SCPP model, boundary conditions, and inclination angle (θ). By taking advantage of planar symmetry, 15° CFD model is employed to reduce the computational time of the numerical analysis.

The grid is generated employing ANSYS Meshing in Figure 1(b). The unstructured tetrahedral mesh is applied for the numerical simulation because this grid is more appropriate and effective for the complex geometry and generated with fewer cells compared to the hexahedral mesh. A growth rate of 1.2 is specified to adjust the mesh transition between the layers of tetrahedral elements. The quality of the mesh is evaluated in terms of different mesh quality metrics such as the orthogonal quality, skewness, and aspect ratio. In this study, the minimum orthogonal quality value is 0.22; maximum skewness and aspect ratio values are 0.93 and 10, respectively. They are within acceptable range [21, 22]. Most of the orthogonal quality and skewness values have a very good range of 0.7-0.95 and an excellent range of 0-0.25, respectively. Thus, the overall quality of the grid in this study is considered to be good.

Changing chimney, collector, and ground (absorber) geometry of SCPP of Manzanares is active research area to enhance thermal performance and power generation of SCPPs. Mandal et al. [11] studied different chimney and ground shapes by altering chimney divergence angle ϕ (-0.75°-3°), ground slope angle of absorber γ (0°-0.6°), and chimney outer diameter (sudden expansion and contradiction). Also, they presented different absorber geometry like a stair-shaped [12] and wavy triangular [13].

In the study, the new chimney geometries are generated by altering chimney entrance slope (θ = 50°-80°) as shown in Figure 2.

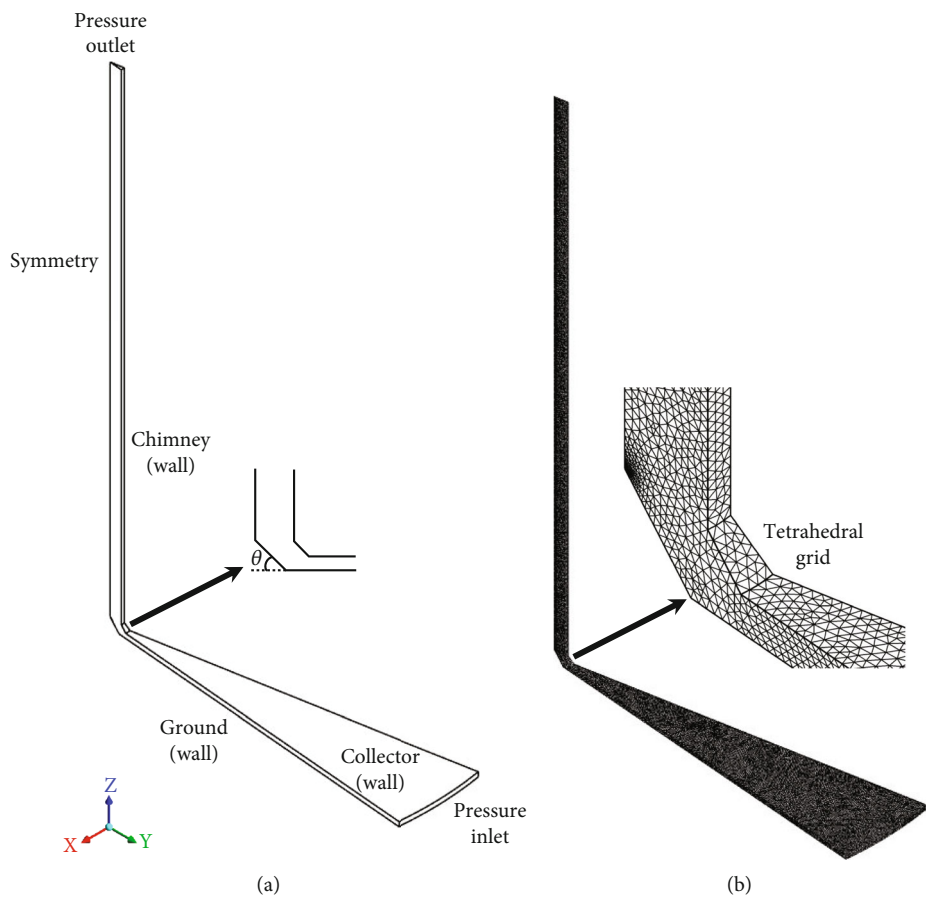

Figure 1: (a) Computational model, boundary conditions, and inclination angle; (b) grid structure of the model.

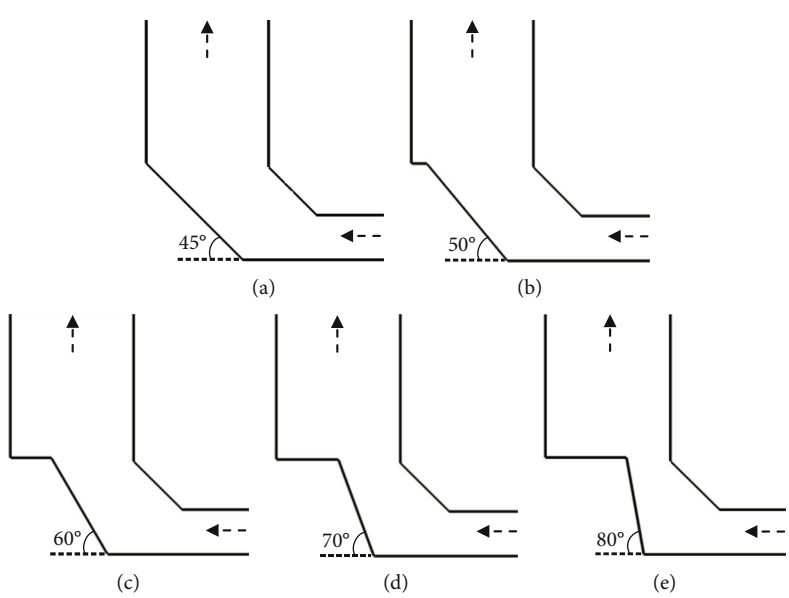

Figure 2: The schematics of the new configurations with different inclination angles: (a) the base, (b) 50°, (c) 60°, (d) 70°, and (e) 80°.

The fillet is a 45° angle. The size of the chimney, collector, and fillet remains fixed for all configurations as shown in Figure 2. Elevating θ causes reducing chimney entrance area. The innovative configurations in Figure 2 have not been considered before by researchers for assessing the performance of SCPP.

Air inside the SCPP system is presumed to follow the ideal gas law. The flow is steady state, incompressible, and

turbulent. Due to minor density alteration in the system [23], the Boussinesq model is preferred to evaluate the air density (ρ) in the CFD study [10, 13].

$$(\rho - \rho_a)g \approx -\rho_a \beta (T - T_a), \tag{1}$$

where β is thermal expansion coefficient and ρ_a and T_a are the ambient density and temperature, respectively. $\rho_a = 1.2046\,\mathrm{kg/m^3}$.

The conservation equations [24] together with the turbulence and discrete ordinate (DO) radiation models are discretized using the computational grid and solved utilizing ANSYS Fluent solver based on finite volume method.

The continuity equation is as follows:

$$\frac{\partial}{\partial x}(\rho u) + \frac{\partial}{\partial y}(\rho v) + \frac{\partial}{\partial z}(\rho w) = 0. \tag{2}$$

The momentum equations are as follows:

$$\begin{aligned}
\frac{\partial}{\partial x}(\rho uu) + \frac{\partial}{\partial y}(\rho uv) + \frac{\partial}{\partial z}(\rho uw) &= -\frac{\partial P}{\partial x} + \mu\left(\frac{\partial^2 u}{\partial x^2} + \frac{\partial^2 u}{\partial y^2} + \frac{\partial^2 u}{\partial z^2}\right),\\
\frac{\partial}{\partial x}(\rho vu) + \frac{\partial}{\partial y}(\rho vv) + \frac{\partial}{\partial z}(\rho vw) &= -\frac{\partial P}{\partial y} + \mu\left(\frac{\partial^2 v}{\partial x^2} + \frac{\partial^2 v}{\partial y^2} + \frac{\partial^2 v}{\partial z^2}\right),\\
\frac{\partial}{\partial x}(\rho wu) + \frac{\partial}{\partial y}(\rho wv) + \frac{\partial}{\partial z}(\rho ww) &= -\frac{\partial P}{\partial z} + \mu\left(\frac{\partial^2 w}{\partial x^2} + \frac{\partial^2 w}{\partial y^2} + \frac{\partial^2 w}{\partial z^2}\right).
\end{aligned} \tag{3}$$

The energy equation is as follows:

$$\begin{aligned}
\frac{\partial}{\partial x}\left(Pc_p uT\right) + \frac{\partial}{\partial y}\left(Pc_p vT\right) + \frac{\partial}{\partial z}\left(Pc_p wT\right)\\
= \lambda\left(\frac{\partial^2 T}{\partial x^2} + \frac{\partial^2 T}{\partial y^2} + \frac{\partial^2 T}{\partial z^2}\right).
\end{aligned} \tag{4}$$

RNG $k - \varepsilon$ turbulence model is chosen to estimate the air flow in the solar chimney. This model takes account of the effect of swirl on turbulence to make accurate predictions of swirling flows [22]. The researchers [15, 16, 20, 22, 25, 26] found that the model predictions were consistent with the measurements taken from the Manzanares plant.

The kinetic energy (k) and dissipation rate (ε) equations of this model are as follows [27]:

$$\begin{aligned}
\frac{\partial}{\partial x_i}(\rho k u_i) + \frac{\partial}{\partial t}(\rho k) &= \frac{\partial}{\partial x_j}\left(\mu_{\mathrm{eff}}\alpha_k \frac{\partial k}{\partial x_j}\right) + G_k\\
&\quad + G_b - \rho\varepsilon - Y_M + S_k,\\
\frac{\partial}{\partial x_i}(\rho \varepsilon u_i) + \frac{\partial}{\partial t}(\varepsilon\rho) &= \frac{\partial}{\partial x_j}\left(\mu_{\mathrm{eff}}\alpha_\varepsilon \frac{\partial \varepsilon}{\partial x_j}\right) + C_{1\varepsilon}\frac{\varepsilon}{k}\left(C_{3\varepsilon}G_b + G_k\right)\\
&\quad - C_{2\varepsilon}\rho\frac{\varepsilon^2}{k} - R_\varepsilon + S_\varepsilon.
\end{aligned} \tag{5}$$

Discrete ordinate (DO) radiation model in ANSYS Fluent is employed for solving the radiative heat transfer equation since this model is appropriate for a semitransparent collector [11, 12].

$$\begin{aligned}
\nabla.\left(I\left(\vec{r}, \vec{s}\right)\vec{s}\right) + (a + \sigma_s)I\left(\vec{r}, \vec{s}\right)\\
= \mathrm{an}^2\frac{\sigma T^4}{\pi} + \frac{\sigma_s}{4\pi}\int_0^{4\pi} I\left(\vec{r}, \vec{s}\,'\right)\varpi\left(\vec{s}.\vec{s}\,'\right)d\Omega',
\end{aligned} \tag{6}$$

where I is the radiation intensity; $\vec{r}$, $\vec{s}$, and $\vec{s}\,'$ denote the position, direction, and scattering direction vectors, respectively; a and σ_s present the absorption and scattering coefficients, respectively; and n, ϖ, and Ω' are the refractive index, phase function, and solid angle, respectively.

The ray tracing approach is chosen for the solar load model due to the highly efficient method for employing solar loads in the energy equation. The solar calculator is used to determine the position of solar radiation for the specified time-of-day and date to stimulate Manzanares condition [25]. Latitude and longitude are specified as 38.99° north and 3.37° west, respectively.

The characteristic of the flow in the solar chimney system is estimated by Rayleigh number (Ra), a dimensional parameter defined as follows [28]:

$$\mathrm{Ra} = \frac{g\beta\Delta T L^3}{\alpha\nu}, \tag{7}$$

where g is acceleration owing to gravity, ΔT presents temperature difference, L is the collector height, and α and ν are the thermal diffusion coefficient and kinematic viscosity, respectively. The material properties of the system components are given in Table 2.

SIMPLE solution method is utilized for a pressure-velocity coupling in ANSYS Fluent. The gradient is computed by setting Green-Gauss cell-based method, and PRESTO spatial discretization method is selected for pressure whereas the discretization scheme is second-order upwind for momentum, turbulence, energy and discrete ordinates. The convergence criterion is set as 10^{-4} for the all equations. A solution is considered to be converged when all of scaled residuals are less than these numbers.

2.2. Performance Parameters. The mass flow rate of the air, across the plant, is expressed by the following [22]:

$$\dot{m} = \rho Q, \tag{8}$$

where Q is the air volume flow rate. The turbine pressure drop (ΔP_t) is obtained as shown in the following equation [15]:

$$\Delta P_t = r_t P_t, \tag{9}$$

where the pressure drop ratio of the turbine (r_t) equals 2/3. The average pressure at the turbine (P_t) in Equation (9) is

Table 2: Characteristics of the components utilized in CFD simulation [29].

Properties	Chimney	Collector	Ground
Thermal conductivity (W/mK)	202.4	1.15	1.83
Specific heat (J/kg K)	871	750	710
Density (kg/m^3)	2719	2500	2160
Absorption coefficient	0	0.03	0.9
Emissivity	1	0.9	0.9
Transmissivity	—	0.9	—
Refractive index	1	1.516	1

determined using the calculation results. The turbine is considered to be installed 9 m above the ground [29]. Power output (P_o) is determined by the following equation [29]:

$$P_o = \eta_t Q \Delta P_t, \tag{10}$$

where η_t is the efficiency of the turbine and η_t is taken to be 0.8 [30].

2.3. Boundary Conditions. The boundary conditions applied to the surfaces of the SCPP are given in Figure 1(a). The air is flowing through the collector inlet at 293.15 K, which is imposed as the pressure inlet boundary condition. At the chimney outlet, the air leaves the system at 293.15 K, which is considered as pressure outlet boundary condition. The atmospheric pressure is set at the inlet and outlet. The adiabatic wall boundary condition is assigned to surface of the chimney by setting heat flux (q) to 0 W/m^2. The ground wall is assumed as an opaque wall. The convection thermal boundary condition is employed for the collector surface, and heat transfer coefficient (h) is fixed to 10 W/m^{2}K [15]. The collector is considered as semitransparent. Ambient air temperature is 293.15 K. In order to reduce computational cost, the symmetry boundary condition is applied at two surfaces as shown in Figure 1(a).

2.4. Grid Independence Study. To provide the accurate prediction of airflow in the system, mesh independence check is carried out with three grid sizes consisting of 210210 ($G1$), 314433 ($G2$), and 412501 ($G3$) elements.

The calculated maximum velocity values for three mesh sizes are given in Table 3. The percentage change in the maximum velocity between $G1$ and $G2$ is 3.46% while that between $G2$ and $G3$ is 0.35% in Table 3.

The comparison of the previous results in literature [15, 16, 19–21, 23, 29, 30] indicates that $G3$ can be considered the grid-independent, and thus, this grid is selected for the remaining simulations.

2.5. CFD Model Validation. The model verification is made in comparison to the model predictions with the measurement results of the Spanish solar chimney plant [31] and computational results in the published literature [29, 30, 32, 33] as shown in Figure 3.

Table 3: The results of grid independence test for CFD model.

Cell numbers	Maximum velocity (m/s)	% change
210210	13.88	—
314433	14.36	3.46
412501	14.31	0.35

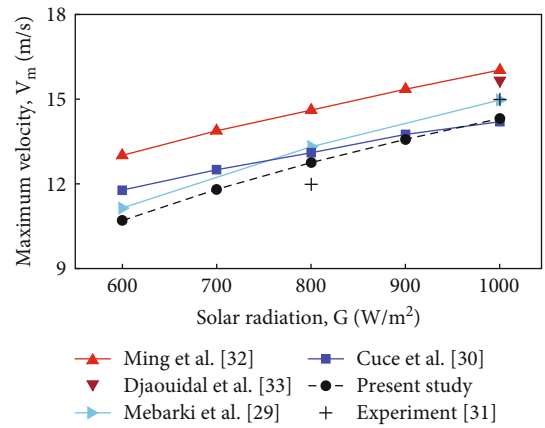

Figure 3: Model validation through comparing maximum velocity of the SCPP model with published experimental and numerical results.

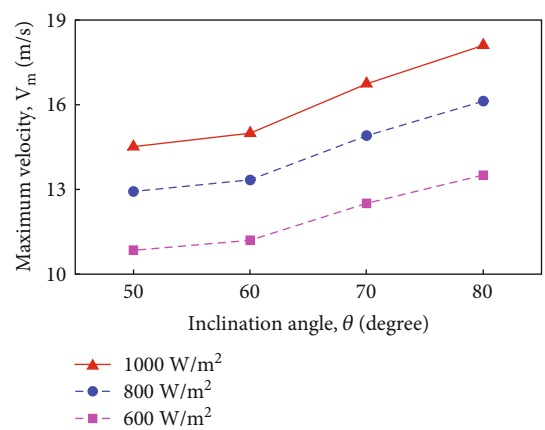

Figure 4: Change of maximum velocity with distinct inclination angles.

Compared to the previous works, the calculated maximum velocity (V_m) values are quite consistent with the experiment at 800 and 1000 W/m^2 as shown in Figure 3. The highest error between the experimental and estimated values is 6.4% at 800 W/m^2. Besides, satisfactory agreement between the present numerical simulation and the computational results is gained by Mebarki et al. [29] and Cuce et al. [30] at 600-1000 W/m^2.

3. Results and Discussion

In this section, detailed discussion about the influences of four distinct chimney inlet configurations on performance

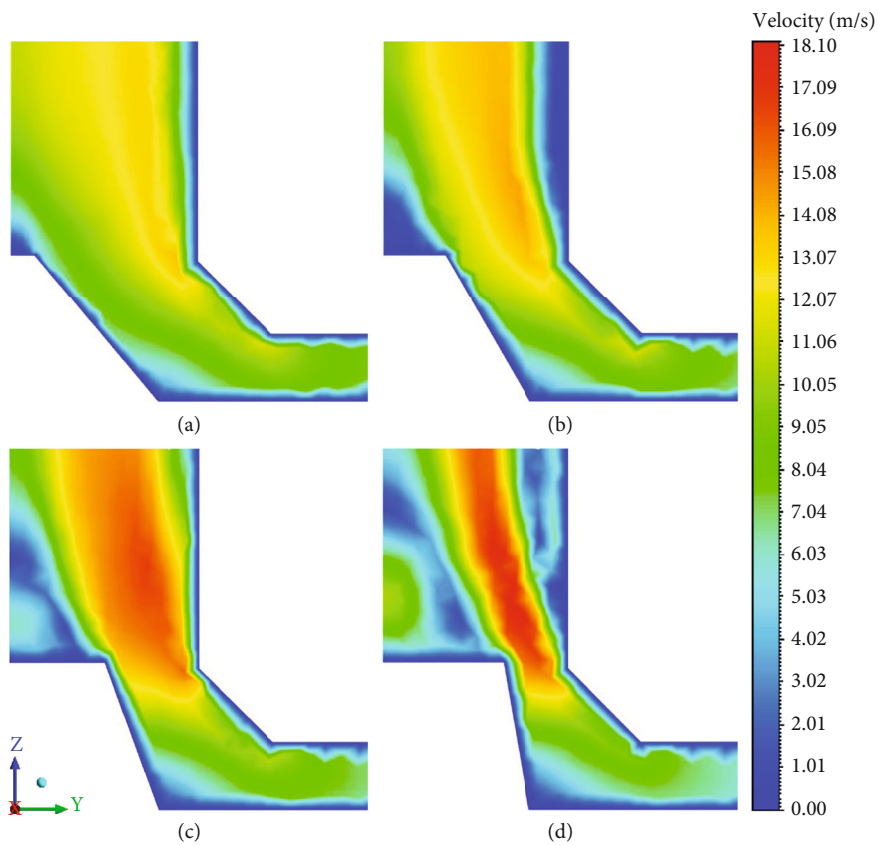

Figure 5: Velocity distribution near the chimney inlet and collector outlet: (a) $\theta = 50^{\circ}$, (b) $\theta = 60^{\circ}$, (c) $\theta = 70^{\circ}$, and (d) $\theta = 80^{\circ}$ at 1000 W/m^2.

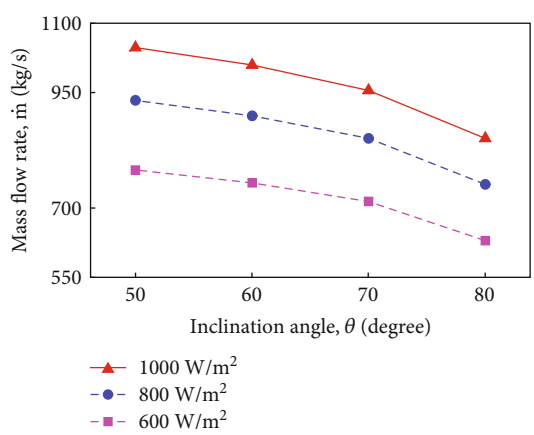

Figure 6: Change of mass flow rate with distinct inclination angles.

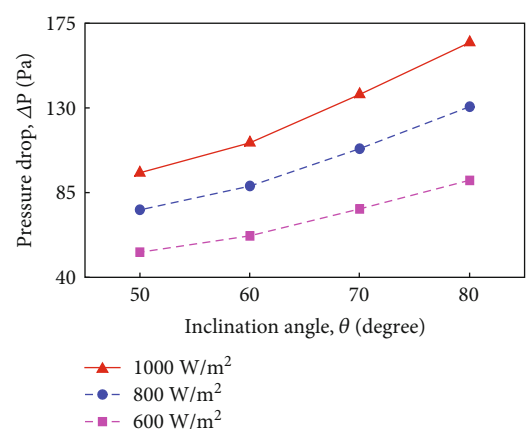

Figure 7: Change of pressure drop with distinct inclination angles.

features of the solar chimney system is presented. The comparisons between the 15° CFD model and the innovative configurations are made via ANSYS Workbench Platform.

3.1. Influence of Various Inclination Angles on Flow and Performance Characteristics. To understand the influence of different inclination angles (50°–80°) on the flow and performance features of the SCPP, the air maximum velocity, mass flow rate, pressure drop in the turbine, and system power output are estimated through the CFD method.

Figure 4 illustrates the change in maximum velocity with various θ at 600-1000 W/m^2. Figure 5 presents the maximum velocity distribution around the chimney entrance and collector outlet for distinct θ at 1000 W/m^2.

It is evident that elevating θ yields a remarkable rise in the maximum velocity in Figure 4. The impact of θ on the maximum velocity is more obvious after $\theta = 60^{\circ}$ at 600-1000 W/m^2.

This is due to a decrease in chimney entrance area with higher θ leading to a highly accelerated flow in this region. The highest air velocity of 18.1 m/s is achieved with $\theta = 80^{\circ}$

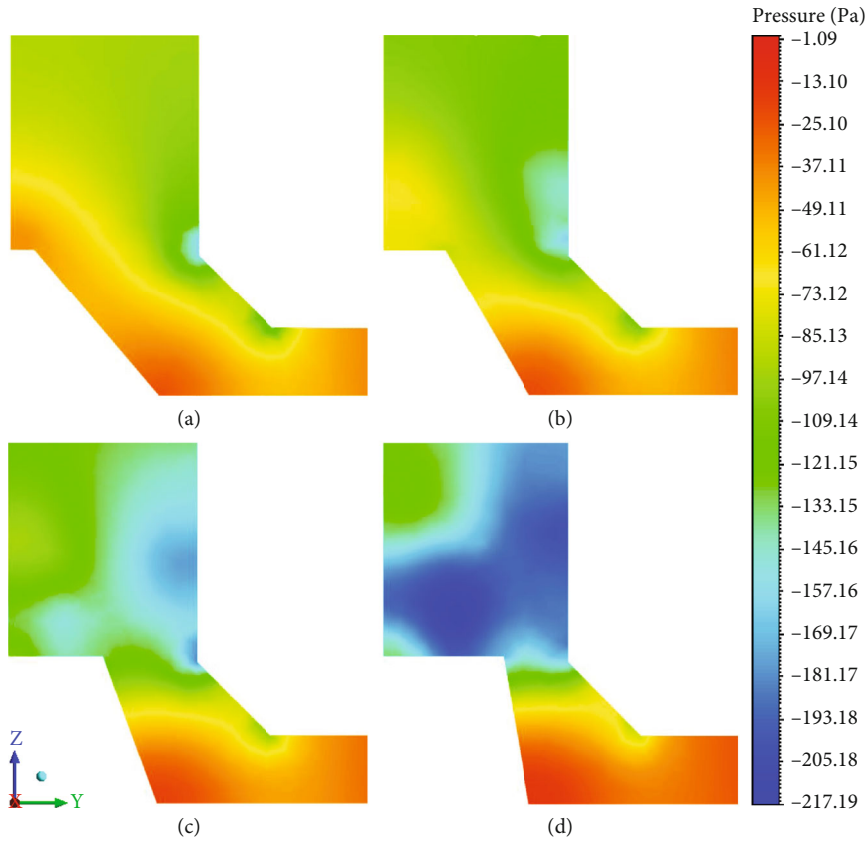

Figure 8: Pressure distribution near the chimney inlet and collector outlet for (a) $\theta = 50^{\circ}$, (b) $\theta = 60^{\circ}$, (c) $\theta = 70^{\circ}$, and (d) $\theta = 80^{\circ}$ at 1000 W/m^2.

at 1000 W/m^2. The maximum velocity is improved by 26.6% in comparison to the base case with $\theta = 45^{\circ}$ producing the maximum velocity of 14.3 m/s at 1000 W/m^2. It is confirmed in the aforementioned result shown in Figure 4 that the augmentation of θ promotes the maximum velocity near the turbine region as shown in Figure 5.

Although velocity distribution is more uniform for $\theta = 50^{\circ}$ as shown in Figure 5(a), higher upward airflow velocity close to the turbine is more important to enhance kinetic energy and pressure difference at the turbine and thus improve the power output [34]. It is observed from Figure 5(d) that the chimney configuration with $\theta = 80^{\circ}$ provides a significant increase in the fluid velocity near the region where the turbine is located compared to others.

The mass flow rate and turbine pressure drop affect the efficiency of the system due to the strong intercorrelation between these parameters. That is, pressure differences across the turbine and the air volume flow rate directly determine power output of the SCPP system as demonstrated in Equation (10). The researchers [8, 9, 35] reveal that both of them are significantly dependent on the geometrical dimensions of the system.

Figure 6 indicates the variation in air mass flow rate with different θ at 600-1000 W/m^2. Figure 7 illustrates the change in turbine pressure drop with different θ at 600-1000 W/m^2.

It is clear in Figure 6 that the air mass flow rate exhibits a decreasing trend with higher θ. The reason for this is that the increase of θ causes a narrower chimney inlet and thus restricts access of air to the chimney. The minimum mass flow rate of 629.5 kg/s is obtained with 80° inclination angle at 600 W/m^2.

The turbine pressure drop has a critical role in designing a solar chimney system and improving the overall system power potential.

A rise in θ leads to a considerable increase in turbine pressure drop at 600-1000 W/m^2 in Figure 7. The highest pressure drop of 164.8 Pa is achieved with the 80° inclination angle configuration at 1000 W/m^2.

Figure 8 presents pressure distribution around the chimney entrance and collector outlet for different θ at 1000 W/m^2. The air in the SCPP system is at negative pressure for all inclination angles as shown in Figure 8. Namely, the pressure inside the plant is less than atmospheric pressure. It is essential to enhancing the pressure potential (difference in pressure between the inward air and atmospheric air) since it is the airflow driving force in the chimney. The findings obtained by four different chimney entrance configurations in Figure 8 indicate that pressure drop considerably augments near the chimney entrance compared to that around the collector outlet.

This explains why the turbine is mounted at a certain height from the base. The change in the inclination angle has a significant impact on the pressure distribution in the chimney, and the dramatic variation of pressure is detected with higher inclination angle configurations, especially for 80° inclination angle as shown in Figure 8(d). As mentioned

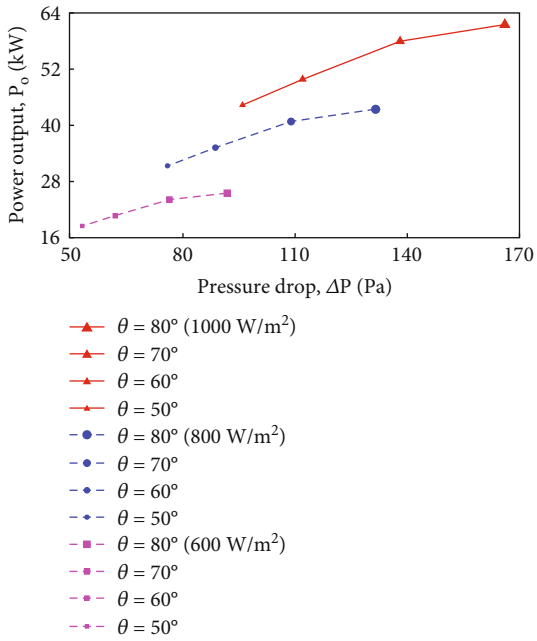

Figure 9: The impact of the inclination angle and pressure drop on the power output at 600-1000 W/m^2.

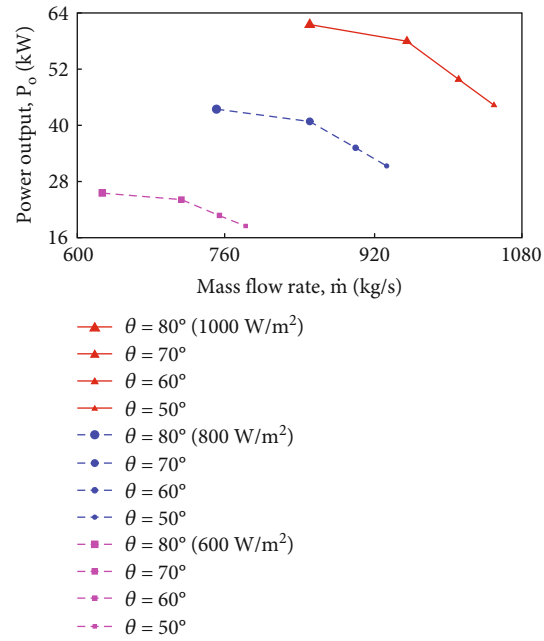

Figure 10: The impact of the inclination angle and mass flow rate on the power output at 600-1000 W/m^2.

earlier, the increase of θ produces a smaller chimney entrance and thus induces nonuniform pressure inside the chimney.

The increment in turbine pressure drop also results in the barrier effect to the air flow within the SCPP. This helps to decrease air mass flow rate with high θ. In addition, the configuration with $\theta = 80^\circ$ has an advantage over others since lower mass flow rate obtained by this configuration contributes to intensify the energy storage performance of the system.

A shape optimization has a key role in performance enhancement of SCPPs [36]. It is concluded that the configuration with 80° inclination angle is a good option to make the system more efficient compared to the base case.

Figure 9 indicates the impact of the change in inclination angle and pressure drop through turbine on the power output of the system at 600-1000 W/m^2.

Figure 10 demonstrates the impact of the change in the inclination angle and mass flow rate on the power output at 600-1000 W/m^2. As mentioned before, pressure difference close to the chimney base where the turbine is situated is the major factor for achieving the highest power output.

The system power output shows an increasing trend with an increase in turbine pressure drop for higher θ at 600, 800, and 1000 W/m^2 shown in Figure 9.

On the other hand, mass flow rate reduces with a rise in θ and a decrease in solar radiation results in further reduction in mass flow rate as seen in Figure 10.

The highest power output of 61.5 kW is achieved with the configuration having 80° inclination angle. In this configuration, power output of the system is improved by 24.5% in comparison to the base case with a power output of 49.1 kW. It is apparent that the rise of θ provides the maximum velocity, turbine pressure drop, and power output enhancements at the expense of reduction in mass flow rate.

It appears that pressure drop through the turbine has a pivotal role in raising the system output power.

4. Conclusions

A 3D model is performed to analyse the impact of the inclination angle (θ) varying in the range of 50°–80° on flow characteristics and power generation of SCPPs by employing DO radiation model combined with RNG $k-\varepsilon$ turbulence model at 600-1000 W/m^2 via the software ANSYS-Fluent. After testing three different meshes for the grid independence solution, the model predictions are verified by comparison with Manzanares pilot plant's measurements. The concluded points based on the CFD simulation are listed as follows:

(i) The 15° computational model with two planar symmetry planes is confirmed by the data of experimental SCPP system in Manzanares, and a reasonably good agreement is observed between measurement and predictions at 800 and 1000 W/m^2 compared to the related numerical works in the literature

(ii) The change in θ leads to the alterations in the flow and performance parameters like maximum velocity, turbine pressure drop, mass flow rate, and power output of the plant. The primary reason for this is that a higher θ produces a narrower chimney entrance leading to airflow limitation around to the chimney inlet

(iii) The air maximum velocity enhances with an increase in θ. The peak air velocity of 18.1 m/s is gained with the 80° inclination angle configuration at 1000 W/m^2. This configuration significantly intensifies upward airflow velocity near the region where turbine is installed and improves the maximum velocity by 26.6% compared with the base model having $\theta = 45^\circ$ producing the peak velocity of 14.3 m/s for 1000 W/m^2 solar radiation

(iv) A rise in θ results in a remarkable increase the turbine pressure drop at 600-1000 W/m^2. The maximum turbine pressure drop of 164.8 Pa is accomplished by the configuration with $\theta = 80^\circ$ at 1000 W/m^2, and this configuration induces strong pressure gradient and thus causes acceleration of the flow close to the chimney entrance

(v) Power generation in the SCPP is highly dependent on the interaction between turbine pressure drop and the air volumetric flow rate as illustrated in Equation (10). The results reveal that power output enhancement in the system is primarily dominated by the turbine pressure drop

(vi) The power output of the system reaches a highest value of 61.5 kW and enhances by 24.5% for $\theta = 80^\circ$ at 1000 W/m^2 in comparison to the base case with power output of 49.1 kW

(vii) The original chimney configurations proposed in the present study can aid in designing an efficient solar chimney plant to elevate the flow and power performance features of the SCPP

Data Availability

The numerical data used to support the findings of this study are included within the article.

Conflicts of Interest

The author has no conflicts of interest to declare.

References

[1] T. Ming, W. Liu, Y. Wu, J. Gui, K. Peng, and T. Pan, *Solar Chimney Power Plant Generating Technology*, Academic Press, London, UK, 1st edition, 2016.

[2] E. Hossain, *The Sun, Energy, and Climate Change*, Springer, Cham, Switzerland, 1st edition, 2023.

[3] A. Rachid, A. Goren, V. Becerra, J. Radulovic, and S. Khanna, *Solar Energy Engineering and Applications*, Springer, Cham, Switzerland, 1st edition, 2023.

[4] C. Mebarki, E. Djakab, A. M. Mokhtari, Y. Amrane, and L. Derradjid, "Improvement of daylight factor model for window size optimization and energy efficient building envelope designs," *Journal of Daylighting*, vol. 8, no. 2, pp. 204–221, 2021.

[5] A. B. Kasaeian, S. Molana, K. Rahmani, and B. Wen, "A review on solar chimney systems," *Renewable and Sustainable Energy*, vol. 67, pp. 954–987, 2017.

[6] M. J. Saleh, F. S. Atallah, S. Algburi, and O. K. Ahmed, "Enhancement methods of the performance of a solar chimney power plant: review," *Results in Engineering*, vol. 19, article 101375, 2023.

[7] M. H. Ali, Z. Kurjak, and J. Beke, "Modelling and simulation of solar chimney power plants in hot and arid regions using experimental weather conditions," *International Journal of Thermofluids*, vol. 20, article 100434, 2023.

[8] E. Cuce, P. M. Cuce, S. Carlucci et al., "Solar chimney power plants: a review of the concepts, designs and performances," *Sustainability*, vol. 14, no. 3, p. 1450, 2022.

[9] P. Das and C. V. Parvathy, "A critical review on solar chimney power plant technology: influence of environment and geometrical parameters, barriers for commercialization, opportunities, and carbon emission mitigation," *Environmental Science and Pollution Research*, vol. 29, no. 46, pp. 69367–69387, 2022.

[10] D. K. Mandal, S. Pradhan, R. Chakraborty, A. Barman, and N. Biswas, "Experimental investigation of a solar chimney power plant and its numerical verification of thermophysical flow parameters for performance enhancement," *Sustainable Energy Technologies and Assessments*, vol. 50, article 101786, 2022.

[11] D. K. Mandal, N. Biswas, N. K. Manna, and A. C. Benim, "Impact of chimney divergence and sloped absorber on energy efficacy of a solar chimney power plant (SCPP)," *Ain Shams Engineering Journal*, vol. 15, no. 2, article 102390, 2024.

[12] N. Biswas, D. K. Mandal, N. K. Manna, and A. C. Benim, "Novel stair-shaped ground absorber for performance enhancement of solar chimney power plant," *Applied Thermal Engineering*, vol. 227, article 120466, 2023.

[13] D. K. Mandal, N. Biswas, A. Barman, R. Chakraborty, and N. K. Manna, "A novel design of absorber surface of solar chimney power plant (SCPP): thermal assessment, exergy and regression analysis," *Sustainable Energy Technologies and Assessments*, vol. 56, article 103039, 2023.

[14] H. Nasraoui, Z. Driss, and H. Kchaou, "Effect of the chimney design on the thermal characteristics in solar chimney power plant," *Journal of Thermal Analysis and Calorimetry*, vol. 140, no. 6, pp. 2721–2732, 2020.

[15] E. Cuce, A. Saxena, P. M. Cuce, H. Sen, S. Guo, and K. Sudhakar, "Performance assessment of solar chimney power plants with the impacts of divergent and convergent chimney geometry," *International Journal of Low-Carbon Technologies*, vol. 16, no. 3, pp. 704–714, 2021.

[16] P. M. Cuce, H. Sen, and E. Cuce, "Impact of tower diameter on power output in solar chimney power plants," *Gazi Journal of Engineering Sciences*, vol. 7, no. 3, pp. 253–263, 2021.

[17] M. A. Aziz and A. M. Elsayed, "Thermofluid effects of solar chimney geometry on performance parameters," *Renewable Energy*, vol. 200, pp. 674–693, 2022.

[18] V. Praveen and V. P. Chandramohan, "Numerical study on optimization of fillet size on the chimney base of solar updraft tower plant for enhanced performance," *Thermal Science and Engineering Progress*, vol. 34, article 101400, 2022.

[19] W. Haaf, K. Friedrich, G. Mayr, and J. Schlaich, "Solar chimneys part I: principle and construction of the pilot plant in Manzanares," *International Journal of Solar Energy*, vol. 2, no. 1, pp. 3–20, 1983.

[20] E. Cuce, P. M. Cuce, and H. Sen, "A thorough performance assessment of solar chimney power plants: case study for

Manzanares," *Cleaner Engineering and Technology*, vol. 1, article 100026, 2020.

[21] P. Das and V. P. Chandramohan, "Effect of chimney height and collector roof angle on flow parameters of solar updraft tower (SUT) plant," *Journal of Thermal Analysis and Calorimetry*, vol. 136, no. 1, pp. 133–145, 2019.

[22] S. R. Keshari, V. P. Chandramohan, and P. Das, "A 3D numerical study to evaluate optimum collector inclination angle of Manzanares solar updraft tower power plant," *Solar Energy*, vol. 226, pp. 455–467, 2021.

[23] M. Saad, N. Ahmed, L. Giovannini, M. Mahmood, M. U. Rafi, and M. A. Qaisrani, "Evaluation of possible integration of solar chimney power plants with high-rise buildings: a numerical analysis," *Journal of Building Engineering*, vol. 60, article 105188, 2022.

[24] W. M. Kays, M. E. Crawford, and B. Weigand, *Convective Heat and Mass Transfer*, McGraw-Hill, Boston, USA, 4th edition, 2005.

[25] A. Hassan, M. Ali, and A. Waqas, "Numerical investigation on performance of solar chimney power plant by varying collector slope and chimney diverging angle," *Energy*, vol. 142, pp. 411–425, 2018.

[26] A. A. Hachicha, E. M. Abo-Zahhad, S. Oh, S. Issa, and S. M. A. Rahman, "Numerical investigation and optimization of a novel hybrid solar chimney for air pollution mitigation and clean electricity generation," *Applied Thermal Engineering*, vol. 226, article 120271, 2023.

[27] ANSYS Fluent, *Theory Guide Release 19.2*, ANSYS Inc., Canonsburg, Pennsylvania, USA, 2018.

[28] S. Pradhan, R. Chakraborty, D. K. Mandal, A. Barman, and P. Bose, "Design and performance analysis of solar chimney power plant (SCPP): a review," *Sustainable Energy Technologies and Assessments*, vol. 47, article 101411, 2021.

[29] A. Mebarki, A. Sekhri, A. Assassi, A. Hanafi, and B. Marir, "CFD analysis of solar chimney power plant: finding a relationship between model minimization and its performance for use in urban areas," *Energy Reports*, vol. 8, pp. 500–513, 2022.

[30] E. Cuce, H. Sen, and P. M. Cuce, "Numerical performance modelling of solar chimney power plants: influence of chimney height for a pilot plant in Manzanares, Spain," *Sustainable Energy Technologies and Assessments*, vol. 39, article 100704, 2020.

[31] R. Rabehi, A. Chaker, Z. Aouachria, and M. Tingzhen, "CFD analysis on the performance of a solar chimney power plant system: case study in Algeria," *International Journal of Green Energy*, vol. 14, no. 12, pp. 971–982, 2017.

[32] T. Ming, W. Liu, and G. Xu, "Analytical and numerical investigation of the solar chimney power plant systems," *International Journal of Energy Research*, vol. 30, no. 11, pp. 861–873, 2006.

[33] B. Djaouida, Z. Aouachria, A. H. Benmachiche, and S. Ali, "Controlling power output of solar chimney power plant according to demand," *International Journal of Ambient Energy*, vol. 41, no. 13, pp. 1467–1481, 2020.

[34] P. Guo, J. Li, Y. Wang, and Y. Liu, "Numerical analysis of the optimal turbine pressure drop ratio in a solar chimney power plant," *Solar Energy*, vol. 98, pp. 42–48, 2013.

[35] E. Cuce, P. M. Cuce, H. Sen, K. Sudhakar, U. Berardi, and U. Serencam, "*Impacts* of ground slope on main performance figures of solar chimney power plants: a comprehensive CFD research with experimental validation," *International Journal of Photoenergy*, vol. 2021, Article ID 6612222, 11 pages, 2021.

[36] N. Biswas, D. K. Mandal, S. Bose, N. K. Manna, and A. C. Benim, "Experimental treatment of solar chimney power plant—a comprehensive review," *Energies*, vol. 16, no. 17, p. 6134, 2023.